Available online at www.sciencedirect.com

ScienceDirect

Procedia Manufacturing 48 (2020) 419–427

Procedia MANUFACTURING

www.elsevier.com/locate/procedia

48th SME North American Manufacturing Research Conference, NAMRC 48 (Cancelled due to COVID-19)

Machinability Of Polyamide 6 Under Cryogenic Cooling Conditions

R. Bertolini*, A. Ghiotti, S. Bruschi*

[a]*Dept. of Industrial Engineering, University of Padova, Via Venezia 1, 35131, Padova, Italy*

* Corresponding author. Tel.: +39 049 8276819; fax: +39 049 8276819. E-mail address: rachele.bertolini@unipd.it

Abstract

Machining of polymeric materials can attain interest when the production lot does not justify the cost of molds or extrusion dies, or when the product to be manufactured requires dimensional accuracy not achievable otherwise. In this framework, the present study aims at evaluating the machinability of the polyamide 6 as a function of the cooling conditions. Two different cryogenic cooling configurations were adopted, whereas the conventional flood cooling was used as reference for sake of comparison, leading to machining conditions under very different temperature ranges. The polyamide 6 machinability was evaluated in terms of surface integrity (surface roughness, surface defects, crystallinity percentage and hardness) and chip morphology.

Results show that the polyamide 6 has to be cut in a specific temperature range, namely between -20°C to 20°C, in order to get the best surface finish, namely achieving the lowest surface roughness and density of defects. In addition, the cryogenic cooling is proved to produce harder surfaces than the flood condition, but leaving unaltered the polymer crystallinity degree.

Keywords: Cryogenic machining; polymer; surface finish; surface integrity; chip morphology

1. Introduction

Machining of polymeric materials has become more and more widespread in many industrial applications as a consequence of the fact that the ever increasing customization of products can make injection, extrusion, or compression molding processes not economically advantageous in terms of mold manufacturing or the above cited processes may not assure the part required geometrical accuracy [1]. On the contrary, machining processes show several advantages in terms of high accuracy capability as well as inherent flexibility; especially in case of reduced production lots, direct mechanical material removal processes help in saving time and reducing costs because the final shape can be directly machined using just a single operation [2].

Nevertheless, there are only few literature studies dealing with the machining of plastics, especially as concerns the machined surface finish and chip morphology. Kakinuma et al. [3] applied cryogenic cooling to micro-mill the polydimethylsiloxane, which is characterized by a glass transition temperature of -123 °C, to manufacture microfluidic chips. A special jig with a cryogenic chamber was developed, in which the workpiece was fully drowned in liquid nitrogen. They found that the cutting forces were considerably higher when using cryogenic cooling, but a successful manufacture of the chips grooves was obtained. Aldwell et al. [4] studied the effect of the workpiece cooling, by submerging it in liquid nitrogen for 24 h, when machining the ultra-high molecular weight polyethylene, characterized by a glassy transition temperature nearby -120°C. They found that the surface roughness was reduced at cold workpiece temperature compared to the one obtained at room temperature, but the obtained improvement was not so outperforming compared to the other investigated process parameters, namely the rake angle, cutting speed, depth of cut, and tool sharpness. Putz et al. [5] evaluated the effect of using cryogenic cooling when machining elastomers, using dry cutting as baseline for comparison. The elastomers under investigations were characterized by a glass transition temperature of 36°C and a hardness of 69 Shore A. They concluded that, in the case of

10.1016/j.promfg.2020.05.064

cryogenic cooling, the surface integrity was improved, since the feed grooves were clearly visible, whereas not in the dry cut samples. In addition, cryogenic cutting induced the formation of segmented, partly continuous chips, while endless ribbon chips formed during dry turning. Ghosh et al. [6] evaluated the effect of cooling conditions to machine an acrylic-based copolymer, characterized by a glass transition temperature in the range between -20°C and 20°C. They evaluated the surface finish, in terms of roughness and waviness, finding that, when the material was cut within the glassy transition region, very wavy surfaces formed, due to the thermal gradient between the cold surface part and the warm inner inside that induced a movement of the subsurface. When machining at temperatures lower than the glass transition range, the waviness was completely eliminated, and the surface roughness was improved of 40%.

So far, the literature review evidences that the machining performances in case of polymeric workpieces are highly dependent on the chemical and thermo-physical properties of the polymer itself. This highlights the need to correlate the machining performances to the specific polymeric material taken into consideration. Furthermore, in none of the previous studies, an attempt to evaluate the effect of the machining parameters on the surface integrity was made.

In this framework, the present paper evaluates the surface finish and surface integrity of the Polyamide 6 (PA-6) when machined under different cooling conditions. The former was considered in terms of surface roughness and surface defects, whereas the latter in terms of thermal properties and hardness. More specifically, the effect of cryogenic cooling when applying two different cooling configurations was studied for the first time using conventional flood cooling as baseline. Finally, the cutting temperature range needed to obtain the best surface finish of the PA-6 was identified.

2. Viscoelastic behavior of polymers

The theory of viscoelasticity describes how polymers respond to a deformation, in terms of either the time or temperature.

In the time frame, the temperature is considered constant. The relaxation time is defined in relation to the sum of vibrational, rotational and translational movements of a polymer at a given temperature. If the polymer is deformed faster than the relaxation time, it will behave like a solid. On the contrary, if it is deformed slower than the relaxation time, its response will be the plastic deformation. In the intermediate time frames, the polymer shows both types of behavior.

In the temperature frame, the time over which the deformation is applied is kept constant. Temperature rises will increase the vibrational, rotational and translational motions, reducing the time the polymer takes to respond to a strain in a given manner. In the temperature regime, the polymer mechanical properties change as a function of the temperature, as schematically shown in Fig. 1 a). Amorphous polymers exhibit three distinct behaviors, namely glassy state, rubbery plateau, and flow regime. The transition between the glassy and the other states is called glass transition.

Different stress-strain curves correspond to these bulk modulus changes as reported in Fig. 1 b). Specifically, four different mechanical behavior types can be highlighted, namely brittle, ductile or tough, cold flow, and rubbery. In the brittle regime, the material supports a high level of stress, but breaks before yielding. In the ductile or tough regime, the yield point is reached before fracture. In the cold flow regime, high level of stress and strains are sustained by the material. In the rubbery region, the material is characterized by high elongation at fracture and low elastic modulus, as the polymeric chains are obstructed to move past each other for long distances, but short range motions are possible.

The accepted notion is that the best machining performance and the best surface finish are obtained within the cold flow regime. However, since the machinability is highly dependent on the material characteristics, the best temperature window for machinability must be defined for each specific polymer [1].

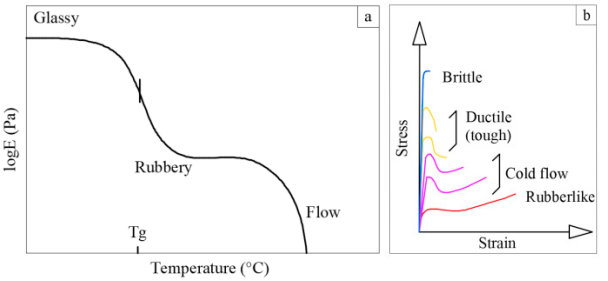

Fig. 1. a) Elastic modulus as a function of temperature, and b) schematic representation of the stress-strain curves within the temperature frame.

Nomenclature

PA-6	Polyamide
T_g	Glass transition temperature
T_m	Melting temperature
T_c	Crystallization temperature
$\dot{Q}$	Cooling capacity
DoC……	Depth of cut
V_c……	Cutting speed
H_c…….	Enthalpy of melting of 100% crystalline PA-6
H_m…….	Enthalpy of melting
X_c……	Percentage of crystallinity
ΔX_c……	Degree of crystallinity compared to the initial condition
S_a……	Surface roughness
S_v……	Maximum valley depth
S_p……	Maximum peak height

3. Experimental

3.1. Material characterization

The material under investigation was the PA-6, whose molecular structure is schematically depicted in Fig. 2.

The material was provided in form of a bar of 40 mm of diameter and 1000 mm of length. Before machining, the bar was subjected to an annealing process at 85°C for 24 h in order to relieve the pre-existing tension within the bar itself.

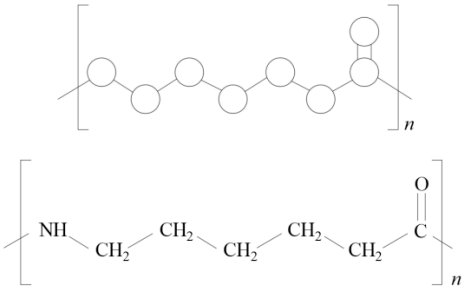

Fig. 2. PA-6 molecular structure.

After annealing, Differential Scanning Calorimetry (DSC) measurements were performed using a DSC™ 200 differential scanning calorimeter to inspect the PA-6 thermal characteristics. A heating-cooling-heating cycle was applied, during which the specimen was continuously heated up to 260°C with a heating/cooling rate of 10°C/min. Fig. 3 a) shows the obtained results, and the relative significant temperatures: crystallization temperature T_c= 187°C, melting temperature T_m= 214°C, and glass transition temperature T_g= 20°C.

FT-IR analyses were carried out using a Jasco™ FT/IR-42000 Fourier Transform Infrared Spectrometer, showing results in a good agreement with the conventional PA-6 structure. The characteristic groups, highlighted by a star on the peaks of Fig. 3 b), are the following: N–H bending vibration in primary amine (3301.81 cm^{-1}), CH stretching of the ethylene sequence (2930.31 and 2861.84 cm^{-1}), C=O amide I stretching (1645.95 cm^{-1}), and the combination absorbance of the N–H and C–N amide II stretching (1551.45 cm^{-1}) [7].

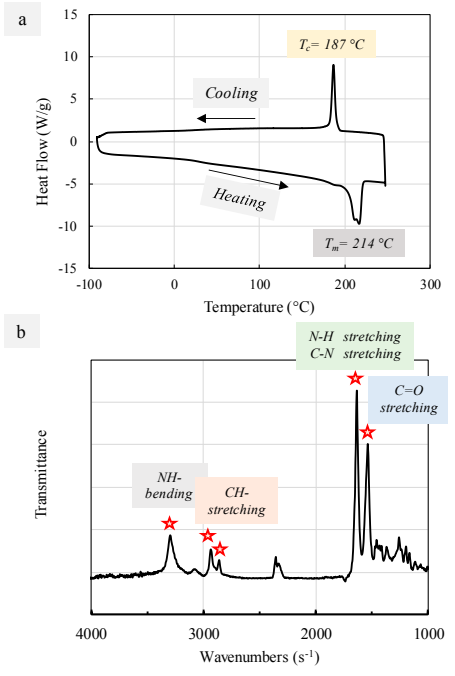

Fig. 3. a) DSC and b) FT-IR results for the PA-6 in the as-delivered state.

3.2. Machining trials

Turning operations were conducted on a NL 1500 Mori Seiki™ CNC lathe. The adopted cutting tool was a semi-finishing insert VCEX110301LF1125 with a radius of 0.1 mm supplied by Sandvik Coromant™. The PA-6 bar was first rough machined to a diameter of 40 mm with the following fixed parameters: cutting speed of 100 m/min, depth of cut of 0.3 mm, and feed of 0.3 mm/rev. Since the feed effect on the surface roughness is well known, multiple finishing passes to reach a final diameter of 35 mm were carried out at constant feed of 0.1 mm/rev. The cutting speed *Vc* and the depth of cut *DoC* were varied according to the experimental plan reported in Table 1.

Table 1. Experimental plan for the machining campaign.

Test ID	DoC (*mm*)	V_c (*m/min*)
1	0.25	50
2	0.25	100
3	0.25	200
4	0.5	200
5	1	200

In order to identify the optimal process window for the PA-6, two different cryogenic cooling configurations were investigated. In the first one, called hereafter "Cryo_1, a single nozzle, directed on just the tool flank face, was used, spraying liquid nitrogen at a pressure of 15 bar.
In the second configuration, called hereafter "Cryo_2", two copper nozzles of 0.9 mm diameter were directed simultaneously on the tool flank and rake faces and sprayed liquid nitrogen at the same pressure of the other configuration. This configuration stands for the classical one, adopted in many other research studies [8, 9].

The cooling capacity of a lubricant was defined in [10], taking into account all the variables that play a role into conditioning the temperature during cutting operations. In the present study, both the temperature and the pressure of the sprayed liquid nitrogen were kept fixed, whereas the number of the nozzles was changed. The cooling capacity, expressed in (kW), is defined according to Eq. (1):

$$\dot{Q}=\dot{m}Q \tag{1}$$

where $\dot{m}$ represents the mass rate (kg/s), and Q the heat exchanged by the system with the environment (kJ). The calculation of the abovementioned parameters was carried out according to the procedure described in [10]. Table 2 reports the cooling capacities of the two different cryogenic cooling configurations used in this study, showing that the Cryo_1 cooling capacity was halved compared to the Cryo_2 one.

Table 2. Mass rate and cooling capacity for the adopted cryogenic cooling configurations.

Cooling configuration	$\dot{m}$ (kg/s)	$\dot{Q}$ (kW)
Cryo_1	0.029	12.35
Cryo_2	0.058	24.7

The standard conventional flood, called hereafter "Flood", was chosen as baseline for comparison. It refers to the use of a standard commercial semi-synthetic oil (Monroe™ Astro-Cut HD XBP) mixed with water (1:20 mixing ratio). In this regime, the oil is sprayed without any kind of regulation onto the cutting zone.

Temperature during cutting was measured by means of the infrared thermo-camera FLIR™ A6000-series. Since multiple finishing passes were used to obtain the final diameter, enough turning length was assured in order to let the temperature reach a steady state condition.

After machining, the chips were collected and cleaned in an ultrasound bath to remove oil residues. First, a macroscopic analysis of the chip morphology was carried out using a Leica™ DMRE optical microscope equipped with a high definition digital camera with a magnification of 50X. Later on, the chips were inspected using a FEI™ QUANTA 450 Scanning Electron Microscope (SEM) with the Secondary Electron (SE) probe. SEM images were acquired at a magnification of 500X, for each cutting condition.

All the experiments and analyses were conducted three times, and, for each investigated parameter, the average was calculated and considered.

3.3. Surface integrity characterization

The machined surfaces were evaluated using a Sensofar PLu Neox™ optical profiler with a 20x magnification Nikon™ confocal objective. Evaluation of the areal surface texture parameters was performed according to ISO 25178-2:2012.

The surface appearance was inspected by using the SEM, acquiring images at 100X in different zones of the samples. Before SEM inspection, the samples were gold-coated to make them conductive using a Denton Vacuum^{TM} Desk V machine, with a current of 15 mA for 120 s.

After machining, each sample was also inspected by using the DSC and adopting the same testing parameters indicated in § 3.1. The PA-6 percentage of crystallinity X_C was estimated from the first heating cycle using Eq. (2):

$$Xc = 100 * (\frac{Hm}{Hc}) \quad (2)$$

where H_c is the melt enthalpy of 100% crystalline PA-6 (230 J*g^{-1} from the ATHAS databank [11]), and H_m the PA-6 melt enthalpy derived from the DSC scan. ΔX_c stands for the degree of crystallinity compared to the initial state.

The hardness of the machined samples was measured using a SHORE D™ hardness tester, usually employed for hard polymeric materials. The hardness was measured along the workpiece radius, every 3 mm starting from the surface. The measurements were performed immediately after machining test to avoid the influence of air humidity. The measurements were repeated three times to assure repeatability.

4. Results and discussion

4.1. Chip morphology

Three different chip morphologies were identified on the basis of the SEM images (see examples in Fig. 4), namely continuous (C), serrated (S), and dust (D). Table 3 summarizes the obtained chip morphologies as a function of the cutting conditions.

In the case of flood cooling, continuous chips were always formed regardless of the cutting conditions. On the contrary, in the case of Cryo_1, the chips changed from dust to continuous, whereas, in the case of Cryo_2, from dust to serrated, depending on the cutting conditions.

Fig. 5 reports photos of the lathe at the end of the turning operations carried out with the following process parameters: V_c=200 m/min and DoC = 0.25 mm. A skein of continuous chips tangled around the workpiece is visible in the case of flood condition, whereas a chip free workpiece is visible in the case of Cryo_2. The same scenario, namely the bar free of coiled chips, was achieved for Cryo_1 for the same cutting condition, even if the photo is not reported in Fig. 5. The presence of continuous chips binds machine downtime to remove them, as well as impairs the surface finish of the machined components.

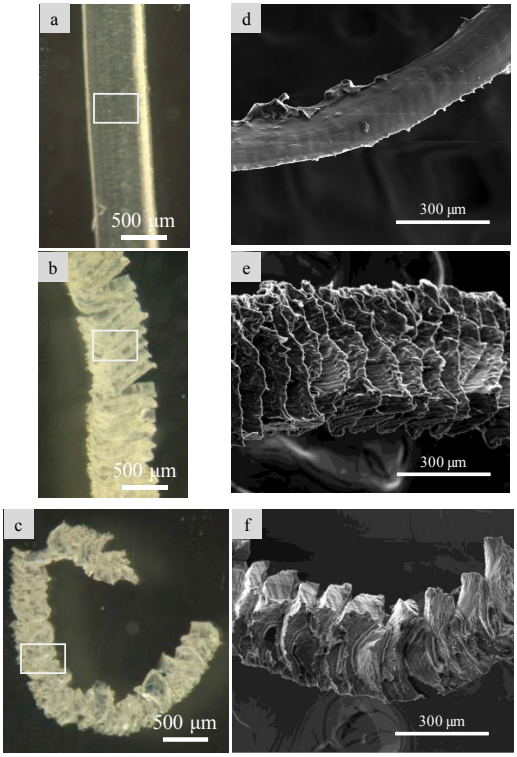

Fig. 4. Different chip morphologies: a) continuous; b) serrated and c) dust and d), e) and f) the corresponding SEM images at a magnification of 400X.

Table 3. Chip morphologies as a function of the cutting conditions (C: continuous, S: serrated, D: dust).

Test ID	DoC (mm)	V_c (m/min)	Flood	Cryo_1	Cryo_2
1	0.25	50	C	D	D
2	0.25	100	C	S	D
3	0.25	200	C	S	S
4	0.5	200	C	C	S
5	1	200	C	C	S

For this reason, chips in form of dust are highly desirable. Segmented chips lie in between the condition of continuous and dust chips, since they tend to tangles like the former, but, at a certain time, they break because of the presence of serrated features, facilitating their evacuation from the lathe (see Fig. 4 d), e) and f)).

The morphology of the chips is strictly correlated to the PA-6 mechanical behavior, which, in turn, is conditioned by the temperature. Fig. 6 reports the temperature values recorded by the infrared thermo-camera during turning as a function of the cutting parameters. In the figure, three different areas are highlighted on the basis of the chip morphologies reported in Table 3. As stated in § 2, at temperatures within the glassy transition temperature range, the material withstands very high strain without breaking. In all the investigated cases, machining in flood condition leads to exceed the T_g, and, therefore, to form continuous chips that cannot break. On the contrary, by using cryogenic cooling, regardless the number of nozzles, the temperatures reached during machining were always lower than the *Tg*, leading the material to behave in a harder way, thus making the chips more prone to break.

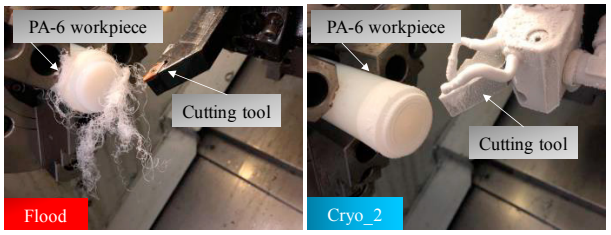

Fig. 5. Lathe at the end of the turning operations with the following process parameters: V_c=200 m/min and DoC = 0.25 mm.

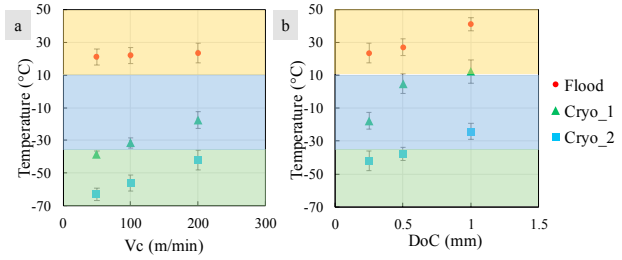

Fig. 6. Recorded temperatures as a function of the cutting conditions.

4.2. Surface finish

The surface roughness as a function of the cutting conditions is reported in Fig. 7. Except for the mildest process parameters, the use of cryogenic cooling always led to the formation of smoother surfaces compared to the flood condition. Moreover, in the case of Cryo_1, the improvement was further enhanced compared to Cryo_2. This proves that the attainment of a certain surface roughness is strictly linked with the temperature reached during machining. In particular, neither too high temperatures nor too low temperatures are beneficial for the surface finish. In fact, Cryo_1, characterized by intermediate cutting temperatures, always led to the formation of the smoothest surfaces.

On the contrary, an evident correlation with the chip morphology could not be highlighted.

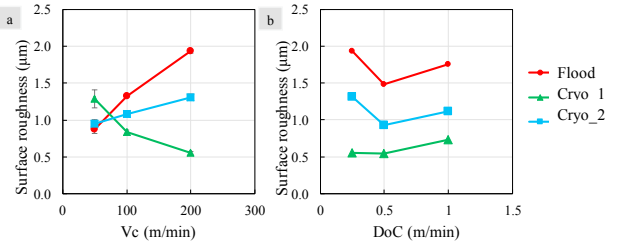

Fig. 7. Surface roughness as a function of the cutting conditions.

In fact, in case of the lowest depth of cut and cutting speed, the flood condition, which was characterized by continuous chips, induced the lowest surface roughness. Similarly, at the lowest depth of cut and intermediate cutting speed, the Cryo_2 was characterized by rougher surfaces than the Cryo_1, even if the former was characterized by chips in the form of dust.

It is worth noting that, in this study, the surface roughness was measured randomly along the specimen thickness, therefore the part of the samples interested by chips entanglements was not specifically evaluated.

Since the surface roughness parameter *Sa* does not give exhaustive information about the presence of defects on the machined surface, other surface texture parameters were taken into consideration, as the maximum valley depth *Sv* and the maximum peak height *Sp* whose values are reported in Fig. 8. These height parameters have already been adopted to measure the amplitude characteristics of defects that could affect workpiece durability [12]. Expect for the test carried out at the lowest depth of cut and cutting speed, the Cryo_2 condition always led to very high values of both *Sv* and *Sp*, indicating the possible presence of defects. On the contrary, in general, the flood and Cryo_1 conditions settled to comparable values, except when the most severe cutting parameters were adopted.

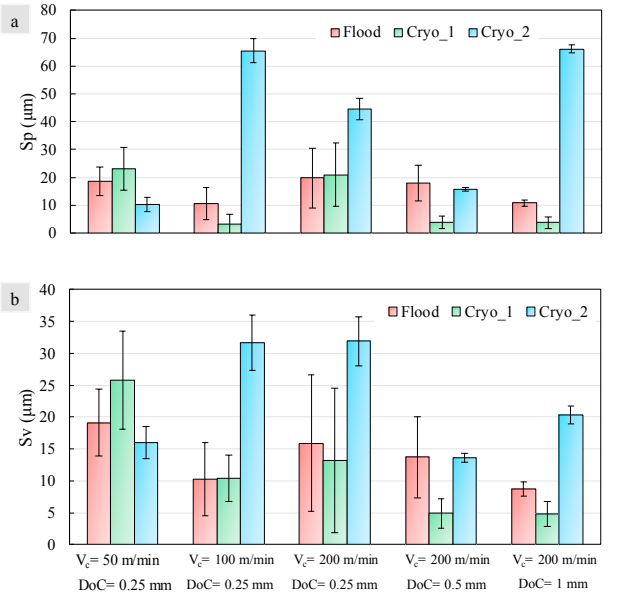

Fig. 8. Maximum peak height (Sp) and maximum valleys depth (Sv) as a function of the cutting conditions.

The SEM images of the machined surfaces reported in Fig. 9 confirm the preliminary considerations using *Sv* and *Sp*. Fig. 9 shows that the main defect present on all the machined surfaces is tearing. Especially for the Cryo_2 sample, the density of tearing was the highest, regardless of the cutting parameters. Furthermore, the defect dimension was the highest when the mildest parameters were used since the cutting temperature was the lowest. In fact, in this condition, the material behaved in a glassy way, leading to the formation of scratches on the surface as a consequence of the mechanism of cutting. This pertains also to the Cryo_1 condition when using the mildest cutting parameters.

However, as the cutting temperature rises, the density of defects gradually decreases, leading to the formation of defects free surfaces when using the most severe cutting parameters for the Cryo_1 condition. Except for the lowest cutting speed and depth of cut, the flood condition always guaranteed the formation of defects free surfaces, due to the poor opposition to the material to be deformed. Anyway, even if higher temperatures promote the formation of defects free surfaces, they contribute to increase the surface roughness value.

4.3. Crystallinity of the machined samples

The T_m, H_m and ΔX_C values, obtained from the first heating cycle portion of the DSC curves, and are reported in Table 4. It can be noted that the PA-6 melting temperature was not affected by any cutting condition.

On the other hand, the enthalpy of melting, and, therefore, the degree of crystallinity was influenced by the cooling conditions. In particular, the crystallinity of the flood cooled specimens was slightly higher compared to the others, especially for the mildest cutting conditions. The increment obtained in the case of flood condition can be attributed to the high temperature reached during the machining process. In fact, crystallinity is a temperature-time dependent parameter. By adopting low cutting speed and depth of cut, the cutting temperature was lower, but the time of cutting was drastically higher favoring the crystallinity increase.

On the contrary, samples machined under cryogenic cooling settled to comparable crystallinity values and did not show significant changes compared to the polymer in the as-delivered state.

Fig. 10 shows an example of the DSC curve obtained as a function of the cooling conditions for the sample machined with Vc=200 m/min and DoC=0.5 mm as representative case for all the cutting parameters. In the case of flood condition, the curve shows the presence of an additional peak at high temperatures, besides the one relative to the melting process. This feature is absent in the case of Cryo_1 and Cryo_2 conditions. The nature of this second peak could be associated with the presence of the impurities inside the material, absorbed during machining. In fact, in both cryogenic configurations, the liquid nitrogen simply evaporates, leaving the workpiece clean.

Fig. 11 shows the crystallinity of the PA-6 machined in flood condition with Vc=100 m/min and DoC= 0.25 mm at the surface, centre and in between. The figure shows that the crystallinity diminishes as a function of the distance from the machined surface, reaching more or less the same value of the material in the as-delivered state.

In fact, the crystallinity reduced from 30.2 % in correspondence of the surface, to 29.5 % at half of the radius, and further to 28.7 % in correspondence of the centre. In addition, the presence of the double peak is visible just at the external surface, confirming the hypothesis of the impurities absorption that might occur at the surface.

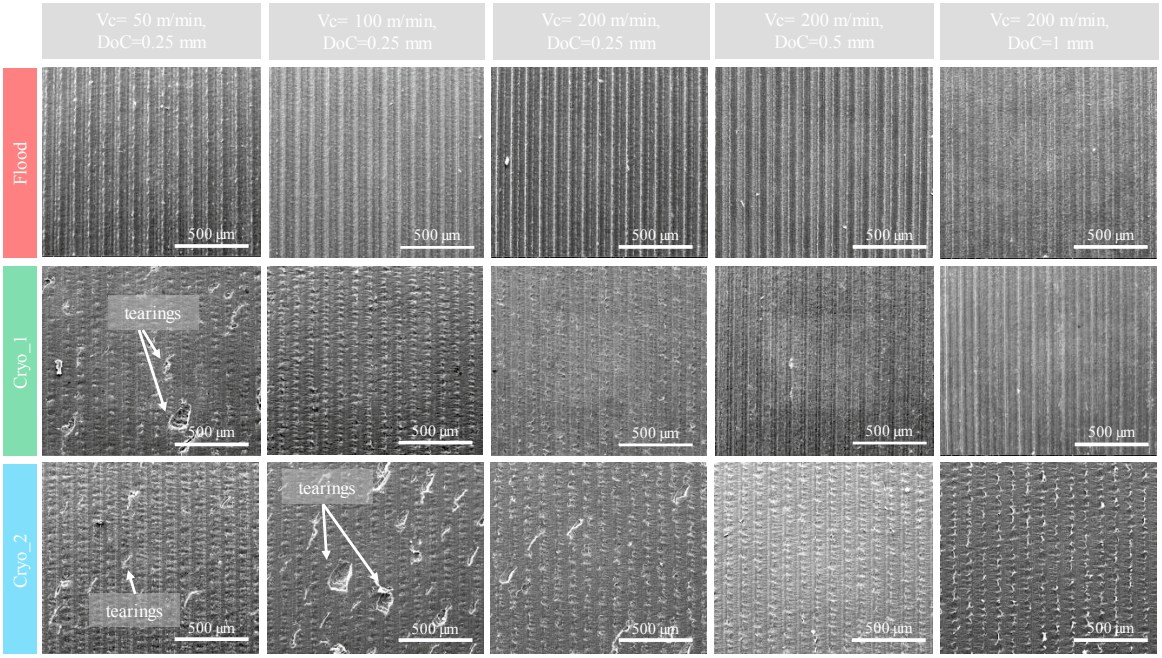

Fig. 9. SEM images of the machined surfaces as a function of the cutting conditions.

Table 4. T_m, E_m and ΔX_C obtained from the DSC first heating cycle.

Test ID	Cooling condition	T_m (°C)	H_m (W/g)	(ΔX_C)
1	Flood	219 ± 5	75 ± 7	10
2	Flood	218 ± 5	79 ± 8	16
3	Flood	218 ± 4	68 ± 8	7
4	Flood	215 ± 1	70 ± 8	3
5	Flood	214 ± 3	68 ± 8	7
1	Cryo_1	214 ± 2	70 ± 7	2
2	Cryo_1	212 ± 4	74 ± 10	4
3	Cryo_1	213 ± 2	70 ± 7	3
4	Cryo_1	214 ± 2	67 ± 1	-1
5	Cryo_1	215 ± 3	70 ± 3	2
1	Cryo_2	215 ± 1	68 ± 8	0
2	Cryo_2	217 ± 4	73 ± 5	1
3	Cryo_2	214 ± 2	70 ± 3	2
4	Cryo_2	215 ± 1	70 ± 1	2
5	Cryo_2	215 ± 1	73 ± 3	1

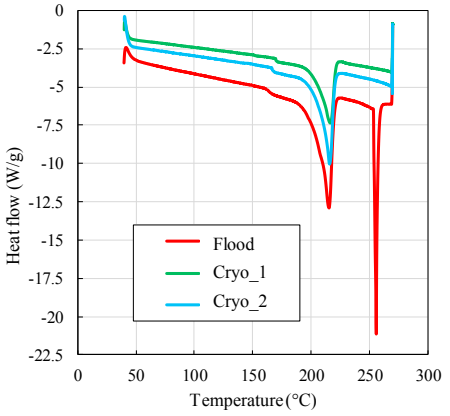

Fig. 10. DSC results as a function of the cooling conditions for samples machined with: V_c=200 m/min and DoC = 0.5 mm.

The polymer crystallinity has a significant effect on the mechanical properties, as shown in Fig. 12 that reports the PA-6 hardness normalized with respect to the initial bulk value, as a function of the distance from the machined surface. In general, the hardness curves show a similar trend, regardless of the cutting conditions.

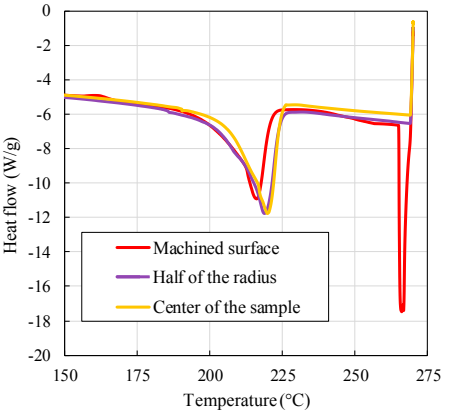

Fig. 11. DSC results as a function of the sample radius for the sample machined under flood condition with: V_c=200 m/min and DoC = 0.5 mm.

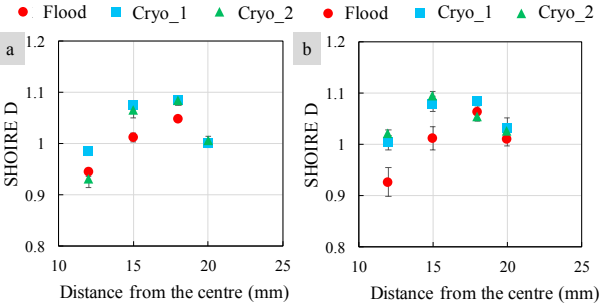

Fig. 12. Hardness as a function of the distance from the sample centre for the samples machined with: a) V_c=200 m/min and DoC = 0.25 mm, and b) V_c=200 m/min and DoC = 0.5 mm.

The hardness gradually decreases as a function of the distance from the machined surface, recovering the as-delivered value approximately at a distance of 8 mm. The main factors affecting the polymer hardness are the distribution and amount of the crystalline and amorphous phases. However, in this case, the amount of crystallinity seems not to have played the major role, since the flood machined samples were characterized by a hardness always lower than the one of the cryogenic machined ones.

5. Discussion

It is generally recognized that lower temperatures induce a glassy behaviour that contributes to the rupture of the chip. The presence of fine particulate swarf is usually associated to micro tears and serrations on the machined surface, which may affect the in-service performances of the product [13]. However, in this study, the surface roughness obtained under Cryo_2 condition, which produced serrated and dust-type chips, was lower compared to the one obtained under at higher temperature relative to turning in flood condition, characterized by continuous chips, as reported in Fig. 7.

The presence of tearings on the surface of the workpiece can impair the functional properties of the workpiece since they can represent a preferential point for subsequent fracture. Fig. 9 evidences the easier formation of this kind of defect when the material is machined at the lowest temperature.

With the aim of improving the quality of the machined parts, surface roughness in combination with surface defects was analysed, and the ideal temperature window for the PA-6 was identified. The classic schematic representation of the polymer stiffness as a function of the temperature with the identification of different regimes was rearranged in Fig. 13 on the basis of the findings of the present study. The definition of the temperature that characterizes the flow region is of great importance, since, as explained in § 2, it represents the optimal machinability window.

The transition point between the tough region and the lower limit of cold flow was recognized as -20°C. In fact, machining with V_c= 200 m/min and DoC= 0.25 mm in Cryo_1 condition led to the lowest roughness among the different cooling conditions, but several amount of defects were still present on the surface (see Fig. 9). This coincides with the change of the

chip morphology from segmented to continuous, meaning that it is strictly connected with the temperature machinability regions. The upper limit of the cold flow region can be recognized as the one that characterized the sample machined with V_c= 50 m/min and DoC= 0.25 mm under flood condition. In fact, this sample was characterized by a rougher surface compared to the one of the Cryo_2 condition, and defects were still present on the machined surface. Finally, the transition between the tough and glassy regions was identified with the change of the chip from segmented to dust, which coincides with the temperature of -40°C.

On the basis of these findings, the temperatures window to obtain desirable surface finish during machining of PA-6 lies in the range between -20°C and 20°C.

The evaluation of the surface integrity showed that the crystallinity in correspondence of the surface was slightly increased in the case of flood condition. This can be explained with the exposition of the material to a temperature higher than the *Tg*, especially when the mildest parameters were used.

The form of the DSC curves also revealed the presence of a characteristic double peak in the case of the flood machined samples, indicating the adsorption of some substances during machining, as a consequence of the intrinsic hygroscopic nature of PA-6.

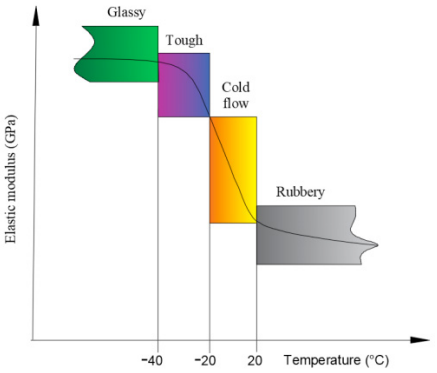

Fig. 13. PA-6 stiffness curve with identification of regions of different machinability.

Crystallization increases the polymer mechanical characteristics, compared to the ones of an amorphous polymer. However, even if the amount of crystallinity is directly linked to the mechanical characteristics, it is not the unique factor affecting them. In fact, from the hardness measurements of Fig. 12 it can be seen that the samples machined under cryogenic conditions were harder compared to the ones machined under corresponding flood conditions. This may suggest that also the residual stresses can play a role, as witnessed by the fact that the maximum hardness increase is obtained in the case of the sample machined with V_c= 50 m/min and DoC=0.25 mm when the material was exposed to the lowest temperature for the maximum time. As a matter of fact, deep cryogenic treatment is often used as a strategy to increase hardness of polymers subjected to wear [14,15].

In addition, the absorption of impurities and oil during machining can have contributed to the softening of the material, as the flood machined samples showed the lowest hardness, regardless of the adopted cutting parameters.

In conclusion, the application of liquid nitrogen can enhance the surface integrity of the PA-6, by avoiding the absorption of oil and contributing to the formation of harder surfaces.

6. Conclusions

The present paper represents the first attempt to evaluate the effect of different cooling conditions on the PA-6 surface finish and surface integrity, the latter in terms of amount of crystallinity and hardness. To this aim, the PA-6 was turned at different cutting speed and depth of cut, adopting different cooling conditions, namely conventional flood and cryogenic cooling, the latter with two different configurations.

The main findings can be summarized as follows:

- The morphology of the chip was strictly related to the temperature reached during machining. The chips changed from continuous to serrated as the temperature decreased below the *Tg,* and from serrated to dust with a further temperature decrease.
- In general, smoother surfaces were obtained when machining in cryogenic cooling conditions than when machining under conventional flood. The best surface finish was obtained by using the cryogenic cooling configuration with a single spraying nozzle.
- It was shown that the morphology of the chip can represent an indirect parameter to prove an excessive cooling of the workpiece leading to a poor surface finish, since the presence of dust chips were indicative of a machined surface of low quality.
- The size and density of the surface defects increased when machining at the lowest temperatures.
- After flood machining, the PA-6 crystallinity slightly increased compared to the as-delivered state, whereas the cryogenic machined sample crystallinity remained unaltered.
- The DSC curves of the flood machined samples proved the absorption of impurities during machining as attested by the presence of a second peak after melting and by local softening in correspondence of the machined surface.
- Cryogenic cooling led to the formation of harder surfaces compared to flood machining, regardless of the adopted cutting parameters.
- The temperature range needed for achieving the best surface finish during turning of PA-6 and the related machinability regions were identified.

References

[1] Carr, JW, Feger C. Ultraprecision machining of polymers. Precision Engineering 1993; 15/4: 221-237.

[2] Song K, Gang MG., Jun MBG., Min B. Cryogenic Machining of PDMS Fluidic Channel Using Shrinkage Compensation and Surface Roughness Control. International Journal of Precision Engineering and Manufacturing 2017; 18/12:1711–17.

[3] Kakinuma Y, Yasuda N, Ayoama T. Micromachining of soft polymer material applying cryogenic cooling. Journal of Advanced Mechanical Design, Systems, and Manufacturing 2008; 2/4: 560-69.

[4] Aldwell B, O'Mahony J, O'Donnell GE. The effect of workpiece cooling on the machining of biomedical grade polymers. Procedia CIRP 2015; 33: 305-310.

[5] Putz M, Dix M, Neubert M, Schmidt G, Wertheim R. Investigation of Turning Elastomers Assisted with Cryogenic Cooling, Procedia CIRP 2016; 40:631–636.
[6] Ghosh R, Knopf JA, Gibson DJ, Mebrahtu T. Cryogenic Machining of Polymeric Biomaterials: An Intraocular Lens Case Study, Medical Device Materials IV: Proceedings of the Materials &Processes for Medical Devices Conference 2008: 1–11.
[7] Kherroub DE, Belbachir M, Lamouri S, Larbi B. Synthesis of Polyamide-6 / Montmorillonite Nanocomposites by Direct In- situ Polymerization Catalysed by Exchanged Clay Synthesis of Polyamide-6 / Montmorillonite Nanocomposites by Direct In-situ Polymerization Catalysed by Exchanged Clay. Oriental Journal of Chemistry 2014; 1429-1436.
[8] Bordin A, Bruschi S, Ghiotti A, Bariani F. Analysis of tool wear in cryogenic turning of electron beam melted Ti6Al4V. Wear 2015; 328: 89-99.
[9] Bermingham MJ, Palanisamy SD. Kent, Dargusch MS, A comparison of cryogenic and high pressure emulsion cooling technologies on tool life and chip morphology in Ti–6Al–4V cutting. Journal of Materials Processing Technology 2012; 212:4:752-65.
[10] Sartori S, Ghiotti A, Bruschi S. Temperature effects on the Ti6Al4V machinability using cooled gaseous nitrogen in semi-finishing turning. Journal of Manufacturing Processes 2017; 30:187–194.
[11] Wunderlich, B. The ATHAS database on heat capacities of polymers. Pure and Applied Chemistry 1995; 67:1019 - 26.
[12] Tailor M, Phaithoonbuathong P, Petzing J, Jackson M., Parkin R. Real-time surface defect detection and the traceable measurement of defect depth in 3D.
[13] Dhokia VG, Newman ST, Crabtree P, Ansell MP. Adiabatic shear band formation as a result of cryogenic CNC machining of elastomers. Proceedings of the Institution of Mechanical Engineers, Part B: Journal of Engineering Manufacture 2011: 1482–1492.
[14] Baldissera P, Delprete C. Current and Potential Applications of Cryogenic Treated Polymers. Springer, Berlin, Heidelberg, 2013. 275-286.
[15] Indumathi J, Bijwe J, Ghosh AK. On the Feasibility of Using Cryo-Treatment as a Tool to Enhance the Abrasive Wear Behaviour of Solid-Lubricated Polymeric Composites. Journal of Synthetic Lubrication 2000; 123–134.